Journal of Mines, Metals and Fuels, *71(10): 1442-1454; 2023. DOI: 10.18311/jmmf/2023/35810*

Print ISSN : 0022-2755

Journal of Mines, Metals and Fuels

Contents available at: *www.informaticsjournals.com/index.php/jmmf*

Three-dimensional Analysis of Electromagnetic Nanomaterial Flow and Thermal Variations for Forced Convection

Sweeti Yadav*, P. A. Dinesh, K. R. Roopa and S. Shashi Prabha Gogate

Department of Mathematics, M S Ramaiah Institute of Technology, Bangalore – 560 054 (Affiliated to Visvesvaraya Technological University, Belagavi – 590 018), India; sweetiyadav1989@gmail.com, dineshdpa@msrit.edu, krroopa870@gmail.com, shashi.jan5@msrit.edu

Abstract

This paper investigates the three-dimensional motion of electromagnetic nanofluid under the influence of heat source/sink, nonlinear heat radiation, magnetic field, and altered Arrhenius equation. Nonlinear stretching in the velocity is considered in the x-direction. Thermophoresis(N_t) and Brownian motion (N_b) are also considered in nanoparticle concentration profiles and temperature analysis. The boundary layer equations are transformed into nonlinear ODEs using suitable similarity transformations. The coupled nonlinear homogeneous system of ordinary differential equations is tackled by the MAPLE software. Non-dimensional system of the equation contains fourteen physical parameters F_r, N_b, M, γ, λ, R_d, δ, Pr, N_t, S, E, Sc, Bi and power index, which are governed by the physical model. Graphs are presented to show the impact of the above-mentioned parameters on temperature, concentration and velocity profile. The present study contributes by observing how the aforementioned parameters influence the heat dissipation rate of nanofluids. This study has broad applications in the field of nanofluids like oil production, metal extrusion, heat exchangers, catalytic reactors etc. Also, results for a particular case found good concurrence with earlier work.

Keywords: *Electromagnetic Radiation, Higher-Order Chemical Reaction, Nanofluid*

1.0 Introduction

Nanofluids are a new class of advanced heat transfer fluids which draw the consciousness of many researchers and industrialists in recent years. Base fluids like water, oil, ethylene glycol, and vegetable oil have less thermal conductivity, making their uses less for industrial purposes. So particles of nano size (less than 10nm) are dispersed in the above base fluids to change their thermal conductivity. The resulting fluid is called nanofluid, which has high thermal properties. Nanomaterials generally used are metal (Al, Cu, Ag, Au, Fe), metal oxide (Al_2O_3, CuO, TiO_2), metal carbide (SiC), Nitride (AlN, SiN), layered (Al+ Al_2O_3, Cu+C), carbon materials (CNTs, diamond, graphite). They increase suspension stability because of their higher surface area than conventional particles. Nanofluids has enormous application in the biomedical industry (sensing and imaging, nano drug delivery, cancer therapeutics, nano cryosurgery), industrial cooling, military applications, nuclear reactor, nanofluid detergent, solar panels, and electronics applications like cooling of microchips. Research on nanofluids has accelerated exponentially since the discovery of the term by Choi[1]. His investigations show the enhancement of the thermal conductivity of nanofluids in the development and applications of Newtonian fluids. Buongiorno[2] explored the main factors of Brownian diffusion and thermophoresis diffusion in the transport of nanofluids.

**Author for correspondence*

Subsequently, this research progressed in other areas like MHD, porous media, nonlinear thermal radiation, viscous dissipation, heat generation, chemical reaction, and Arrhenius energy by various researchers[3-10].

Many real-world problems deal with boundary layer flow caused by stretchable sheets. In many areas, it has applications like hot rolling, paper production, condensation process, artificial fibres, etc. The stretching surface may be linear or nonlinear. The linear stretching surface was first studied by Crane[11] and nonlinear by Khan & Pop[12]. Makinde & Aziz[13] extend this work on the convective boundary condition. The boundary layer flow by a nonlinearly stretching sheet in the presence of thermal radiation and viscous dissipation was first researched by Cortell[14]. Prasad *et al.*[15] and Mukhopadhyay[16] studied heat transfer in a non-isothermal stretching sheet. Vijaya Kumara *et al.*[17] studied convection with porosity in wall heating. Srinvasulu & Bandari[18] examined Arrhenius equation and heat source through a nonlinearly stretching plate. Flows over an unsteady stretching surface considering heat source/sink in an inclined magnetic field was inspected by Elgazery[19]. Jafar *et al.*[20] looked at nonlinear stretching sheets in porous media. Saeed *et al.*[21] examined thin film nanofluid on an inclined stretching surface. Rasool *et al.*[22] numerically investigated nanofluid flow with convective boundary conditions by nonlinear stretching surface. Abbas *et al.*[23] explored the heat transfer properties and the thermal slip of hybrid nanofluid over permeable, nonlinear, curved surfaces.

Porous media improves convective heat transfer, so it is used widely in many applications like enhancement of heat transfer in heat exchangers, water pollution, grain storage, etc. Darcy's theory Darcy[24] is used mathematically with porous media. By Darcy's law, volume flux is directly proportional to the pressure gradient. This law is valid at low flow velocity and weal porosity. Forchheimer[25] extended this law by observing the physical phenomenon. The author included the additional term square velocity to the existing Darcy equation; the final expression is called Darcy- Forchheimer equation. In nanofluids, Darcy- Forchheimer flow is used to analyse the properties of heat transfer. Various studies on Darcy- Forchheimer are pointed out in [26-30]. Along with flow through Darcy-Forchheimer porous media, the following effects are studied convective conditions Muhammad *et al.*[31], ohmic heating and heat source(sink) Upreti *et al.*[32], slip condition Mishra *et al.*[33], electromagnetic field Eid *et al.*[34], thermal radiation and activation energy Sajid *et al.*[35], suction/blowing Alotaibi & Eid,[36]. Radiative heat transfer is used in equipment designing, solar farms, imagining techniques, etc. Shobha *et al.*[37], using the ADI method, tested the influence of nonlinear thermal radiation on Williamson nanofluid. They concluded radiation parameters lower both velocity and temperature. Patil *et al.*[38], checked the impact of radiation parameters on mixed convective hybrid nanofluid through a rotating sphere. They addressed temperature is directly proportional to nonlinear thermal radiation parameters. In [39,40] the nonlinear thermal radiation effect is considered with different physical conditions.

Understanding the importance of work on nanofluids and boundary layer flow caused by stretching sheets carried out by the above-mentioned authors motivates us to extend their research work. This work aims to study the 3-dimensional motion of the electromagnetic fluid through porous extending sheets along nonlinear heat radiation, heat source/sink magnetic field, and altered Arrhenius equation contingent on convective surface boundary conditions. Using appropriate similarity transformation nonlinear system of equations is gained. The numerical solution is determined using MAPLE software. Graphs and tables are constructed for different parameters together with physical justification. The outcomes of this work can be used to improve oil productivity[41], drug delivery[42], radiotherapy, treatment of cancer[43], etc.

2.0 Formulation of Flow Problem

Consider the 3-dimensional motion of nanofluid through Darcy–Forchheimer porous medium accompanying heat radiation, chemical reaction, heat source/sink, thermophoresis, magnetic field and Brownian motion. Magnetic field and fluid motion make an angle of 90^0. The induced magnetic field is inconsiderable. Quadratic stretching in velocity is considered in the x direction and linear stretching in velocity is considered in the y direction. Suction/blowing w_0 is considered on the surface.

Governing equations for the above physical configuration are:

$$\frac{\partial v}{\partial y}+\frac{\partial u}{\partial x}+\frac{\partial w}{\partial z}=0, \qquad (1)$$

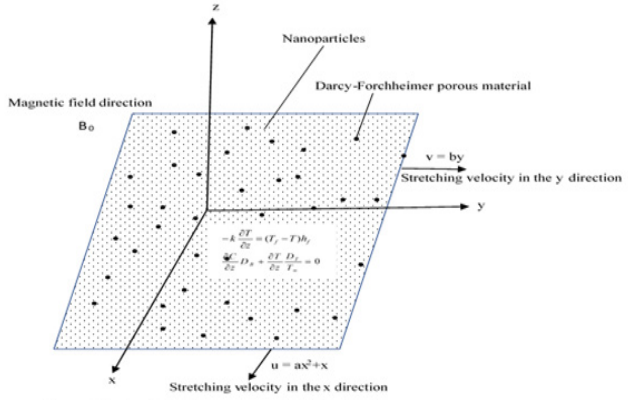

Geometrical model of the nonlinear stretching sheet

$$v\frac{\partial u}{\partial y}+u\frac{\partial u}{\partial x}+w\frac{\partial u}{\partial z}=\frac{\partial^2 u}{\partial z^2}v_f-Fu^2-u\frac{v_f}{K}-u\frac{\sigma B_0^2}{\rho_f}, \quad (2)$$

$$v\frac{\partial v}{\partial y}+u\frac{\partial v}{\partial x}+w\frac{\partial v}{\partial z}=\frac{\partial^2 v}{\partial z^2}v_f-Fv^2-v\frac{v_f}{K}-v\frac{\sigma B_0^2}{\rho_f}, \quad (3)$$

$$v\frac{\partial T}{\partial y}+u\frac{\partial T}{\partial x}+w\frac{\partial T}{\partial z}=\left[D_B\left(\frac{\partial C}{\partial z}\frac{\partial T}{\partial z}\right)+\frac{D_T}{T_\infty}\left(\frac{\partial T}{\partial z}\right)^2\right]\frac{\rho c_p}{\rho c_f}+\alpha^*\frac{\partial^2 T}{\partial z^2}$$

$$-\frac{1}{\rho c_f}\frac{\partial q_r}{\partial z}+\frac{Q}{\rho c_f}(T-T_\infty) \quad (4)$$

$$v\frac{\partial C}{\partial y}+u\frac{\partial C}{\partial x}+w\frac{\partial C}{\partial z}=\left(\frac{\partial^2 C}{\partial z^2}\right)D_B+\left(\frac{\partial^2 T}{\partial z^2}\right)\frac{D_T}{T_\infty}-\exp\left(-\frac{E}{\kappa T}\right)\left(\frac{T}{T_\infty}\right)^m R(C-C_\infty)^n. \quad (5)$$

Considering the geometry of model boundary conditions are given as:

$$v=by,\ u=ax^2+x,\ w=w_0,\ \frac{\partial C}{\partial z}D_B+\frac{\partial T}{\partial z}\frac{D_T}{T_\infty}=0,\ -k\frac{\partial T}{\partial z}=(T_f-T)h_f \ at\ z=0,$$
$$v\to 0,\ C\to C_\infty,\ u\to 0,\ T\to T_\infty \ as\ z\to\infty, \quad (5A)$$

where v - velocity component in the y-direction, -Velocity component in the x-direction and w -velocity component in the z-direction, C - concentration, T - temperature, α^* - thermal diffusivity, v_f- kinematic viscosity, F - porous medium inertia, Q -heat absorption coefficient, D_T - thermophoresis, K- penetrability of the porous medium, ρ_f- density, σ - electrical conductivity, ρc_p- nanoparticle heat capacity, ρc_f - fluid heat capacity, D_B - Brownian motion, C_∞ - ambient concentration, T_∞ - ambient temperature, $\exp\left(-\frac{E}{\kappa T}\right)\left(\frac{T}{T_\infty}\right)^m R(C-C_\infty)^n$ is Arrhenius equation for a chemical reaction where R -reaction rate, k -Boltzmann constant, E - activation energy, n- chemical reaction order, m - rate constant.

Radiative thermal flux given by Roseland approximation is

$$q_r=-\frac{4\sigma^*}{3k^*}\frac{\partial T^4}{\partial z},$$

where σ* - Stefan-Boltzmann constant and k*- absorption coefficient. Using Taylor's series around and T_∞ Roseland approximation, we have

$$\frac{\partial q_r}{\partial z}=-\frac{16\sigma^* T_\infty^3}{3k^*}\frac{\partial^2 T}{\partial z^2}. \quad (6)$$

Applying equation (6), the reduced form of equation (4) is

$$u\frac{\partial T}{\partial x}+v\frac{\partial T}{\partial y}+w\frac{\partial T}{\partial z}=\left[D_B\left(\frac{\partial C}{\partial z}\frac{\partial T}{\partial z}\right)+\frac{D_T}{T_\infty}\left(\frac{\partial T}{\partial z}\right)^2\right]\frac{\rho c_p}{\rho c_f}+$$
$$\left[\alpha^*+\frac{16\sigma^* T_\infty^3}{3k^*(\rho c_p)_f}\right]\frac{\partial^2 T}{\partial z^2}+\frac{Q}{\rho c_f}(T-T_\infty). \quad (6A)$$

Consider the subsequent similarity transformation

$$\varsigma=\sqrt{\frac{a}{v_f}}z,\ v=ayg'(\varsigma),\ u=axf'(\varsigma),\ w=-[f(\varsigma)+g(\varsigma)]\sqrt{a v_f},\ \varphi(\varsigma)=\frac{C-C_\infty}{C_\infty},$$
$$\theta(\varsigma)=\frac{T-T_\infty}{T_f-T_\infty}. \quad (7)$$

The nonlinear system of equations for the partial differential equations (2), (3), (5) and (6A) is given by

$$f'''+f''(f+g)-(M^2+\lambda)f'-f'^2(1+F_r)=0, \quad (8)$$

$$g'''+g''(f+g)-(M^2+\lambda)g'-g'^2(1+F_r)=0, \quad (9)$$

$$\left(1+\frac{4}{3}R_d\right)\theta''+\left[(f+g)\theta'+N_b\varphi'\theta'+N_t\theta'^2+S\theta\right]\Pr=0, \quad (10)$$

$$\phi''+\frac{N_t}{N_b}\theta''+\left[(f+g)\phi'-(1+\delta\theta)^m+\gamma\exp\left(-\frac{E}{\delta\theta+1}\right)\phi^n\right]Sc=0. \quad (11)$$

Applying equation (7), boundary conditions become

$$g(0)=Su,\ g'(0)=\alpha,\ f(0)=0,\ f'(0)=1,\ (N_b\phi'+N_t\theta')(0)=0,$$

$$,\theta'(0)=-Bi[1-\theta(0)],g'(\infty)\to 0,\ f'(\infty)\to 0,\phi(\infty)\to 0,\theta(\infty)\to 0, \quad (11A)$$

where F_r- Forchheimer number, N_t- thermophoresis parameter, λ - permeability parameter, E - activation energy, R_d - radiation parameter, Sc-the Schmidt number, M - magnetic parameter, N_b - Brownian motion parameter, γ - chemical reaction parameter, Pr - Prandtl number, S - the heat absorption/generation parameter and δ - temperature relative parameter. Mathematically, the above parameters are described as follows:

Non-dimensional coefficient of skin friction and Nusselt number are characterized as

$$F_r=\frac{C_b}{\sqrt{K}},S=\frac{Q}{a(\rho c)_f},M^2=\frac{\sigma B_0^2}{a\rho_f},\Pr=\frac{v_f}{\alpha}N_b=D_B\frac{C_\infty}{v_f}\frac{(\rho c)_p}{(\rho c)_f},R_d=\frac{4\sigma^* T_\infty^3}{k^* k},\alpha=\frac{b}{a},$$

$$N_t=\frac{D_T}{T_\infty}\frac{(T_f-T_\infty)}{v_f}\frac{(\rho c)_p}{(\rho c)_f},Sc=\frac{v_f}{D_B}\gamma=\frac{C_\infty^{n-1}R}{a},\delta=\frac{(T_f-T_\infty)}{T_\infty},E=\frac{E_a}{\kappa T_\infty},\lambda=\frac{v_f}{aK'},Bi=\sqrt{\frac{v_f}{a}}\frac{h_f}{k}.$$

$$C_f=\frac{\tau_w}{U_w^2\rho_f},\tau_w=\mu_f\left(\frac{\partial v}{\partial z}\right)_{z=0},$$

$$C_f=\frac{\tau_w}{U_w^2\rho_f},\tau_w=\mu_f\left(\frac{\partial u}{\partial z}\right)_{z=0}, \quad (12)$$

$$Nu=\frac{xq_w}{(T_w-T_\infty)k_f},$$

Using equation (7), equation (12) reduces to

$$C_{fy}\,\mathrm{Re}_y^{\frac{1}{2}}=\alpha^{\frac{-3}{2}}g''(0),$$

$$C_{fx}\,\mathrm{Re}_x^{\frac{1}{2}}=-f''(0),$$

$$Nu_x\,\mathrm{Re}_x^{\frac{-1}{2}}=-\theta'(0),$$

where $\mathrm{Re}=\frac{u.L}{\nu_f}$ is Reynolds number, L is characteristic length.

3.0 Numerical Method and Graphs

For solving highly nonlinear coupled homogeneous differential equations, MAPLE software is used.

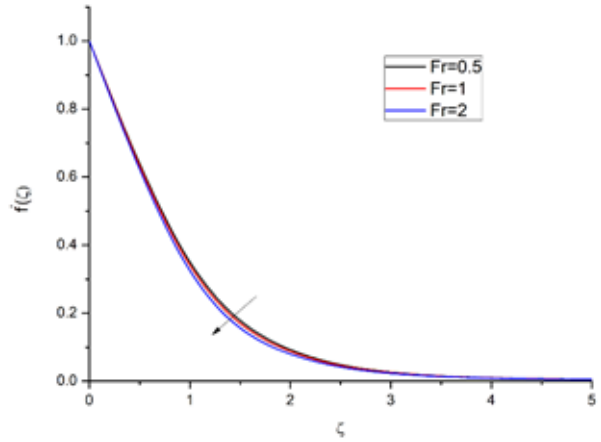

Figure 1. Effect of F_r (Darcy-Forchheimer number) on $f'(\varsigma)$.

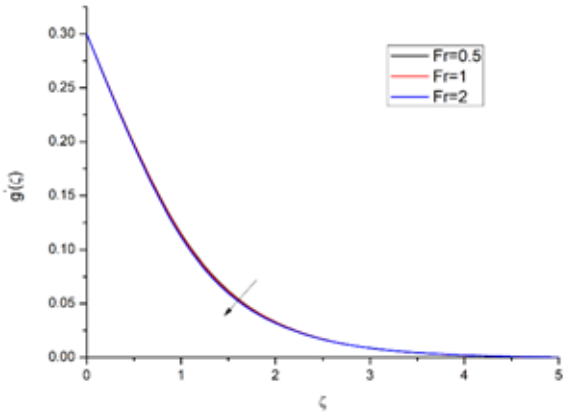

Figure 2. Effect of F_r (Darcy-Forchheimer number) on $g'(\varsigma)$.

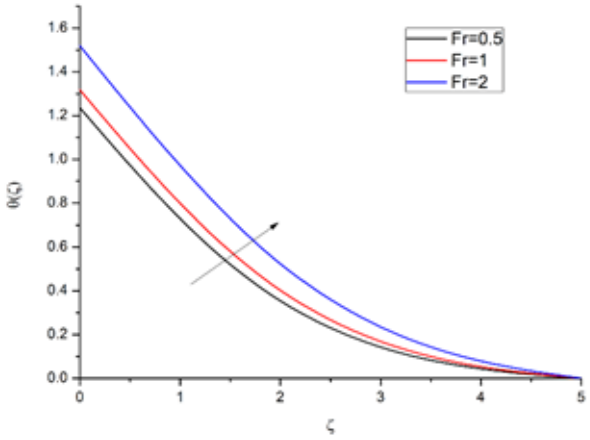

Figure 3. Effect of F_r (Darcy-Forchheimer number) on $\theta(\varsigma)$.

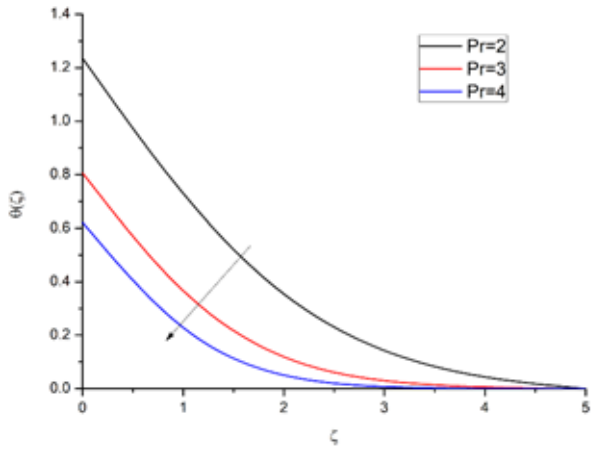

Figure 4. Effect of Pr (Prandtl number) on $\theta(\varsigma)$.

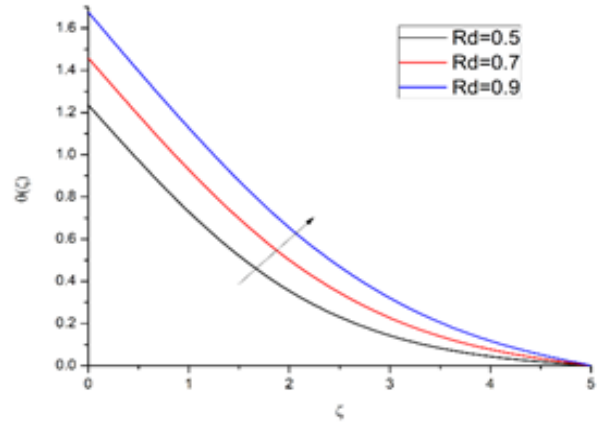

Figure 5. Effect of R_d (radiation parameter) on $\theta(\varsigma)$.

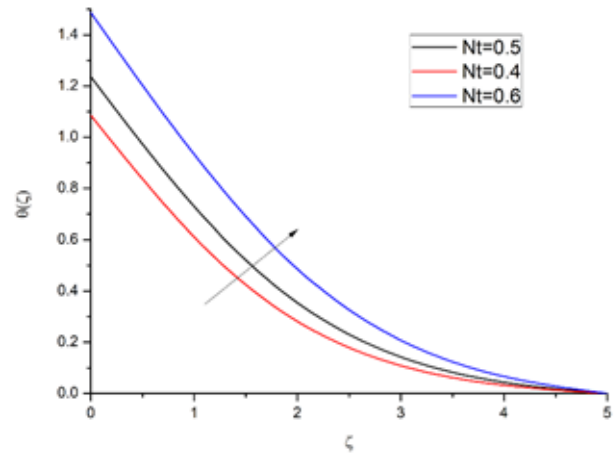

Figure 6. Effect of N_t (thermophoresis parameter) on $\theta(\varsigma)$.

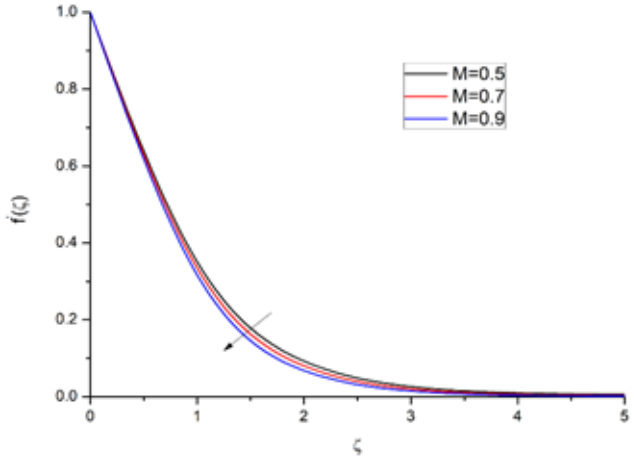

Figure 7. Effect of M (Magnetic parameter) on $f'(\varsigma)$.

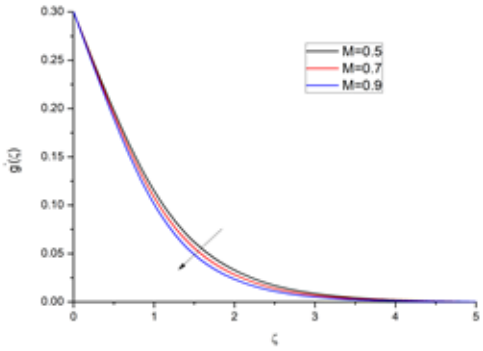

Figure 8. Effect of M (Magnetic parameter) on $g'(\varsigma)$.

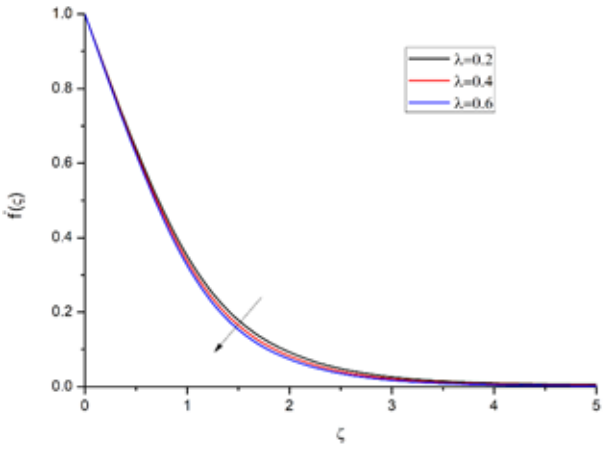

Figure 9. Effect of λ (permeability parameter) on $f'(\varsigma)$

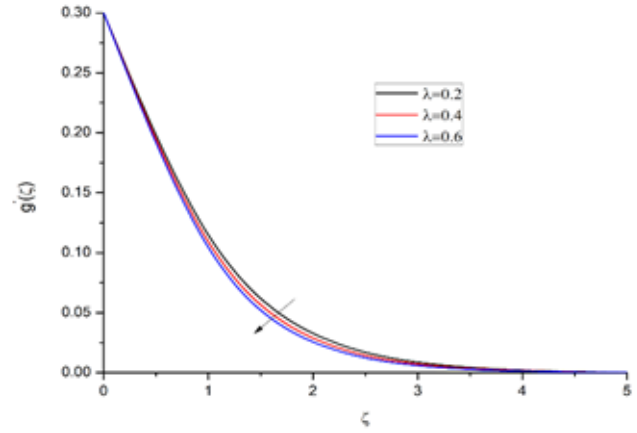

Figure 10. Effect of λ (permeability parameter) on $g^{'}(\varsigma)$.

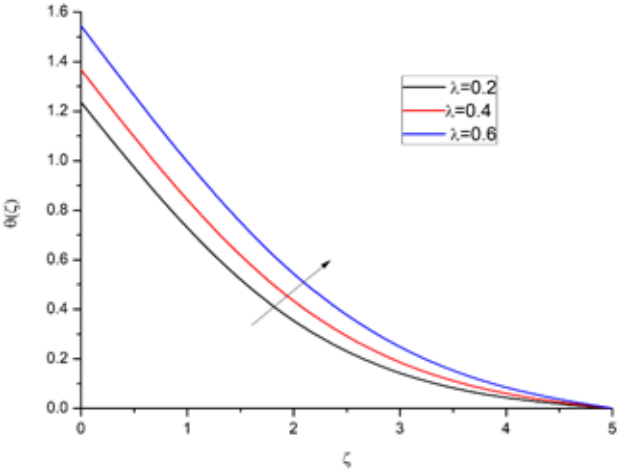

Figure 11. Effect of λ (permeability parameter) on $\theta(\varsigma)$.

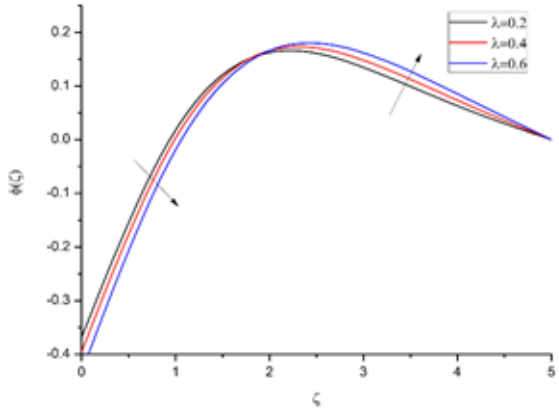

Figure 12. Effect of λ (permeability parameter) on $\varphi(\varsigma)$.

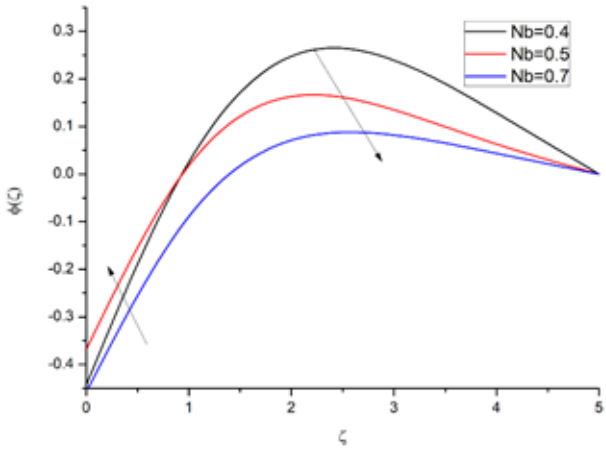

Figure 13. Effect of N_b (Brownian motion parameter) on $\varphi(\varsigma)$.

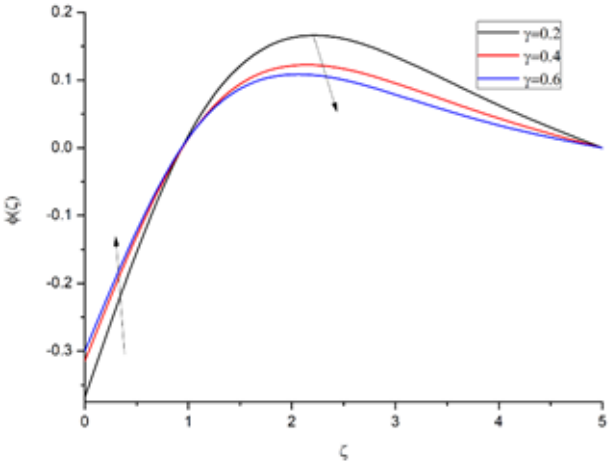

Figure 14. Effect of γ (chemical reaction parameter) on $\varphi(\varsigma)$.

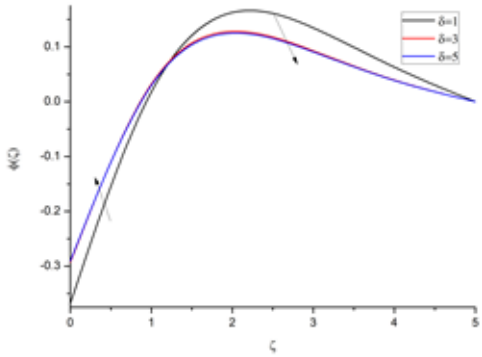

Figure 15. Effect of δ (temperature ratio parameter) on $\varphi(\varsigma)$.

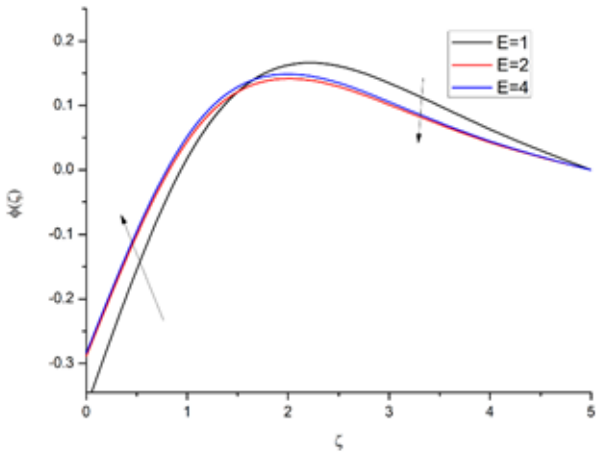

Figure 16. Effect of E (activation energy) on $\varphi(\varsigma)$.

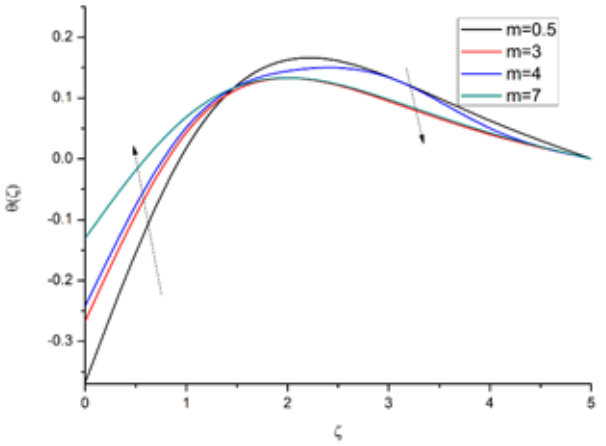

Figure 17. Effect of m (rate constant) on $\varphi(\varsigma)$.

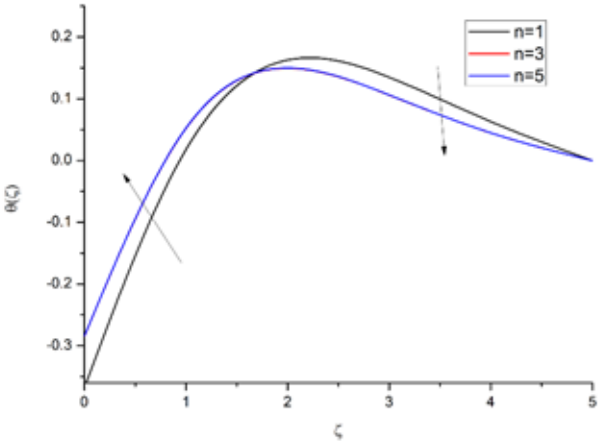

Figure 18. Effect of n (chemical reaction order) on $\varphi(\varsigma)$

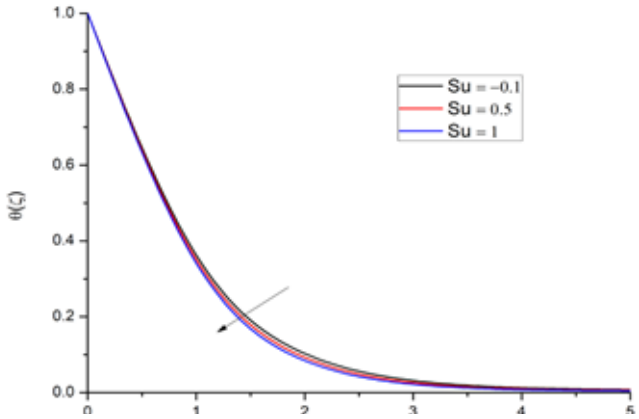

Figure 19. Effect of Su (Suction parameter) on $\theta(\varsigma)$.

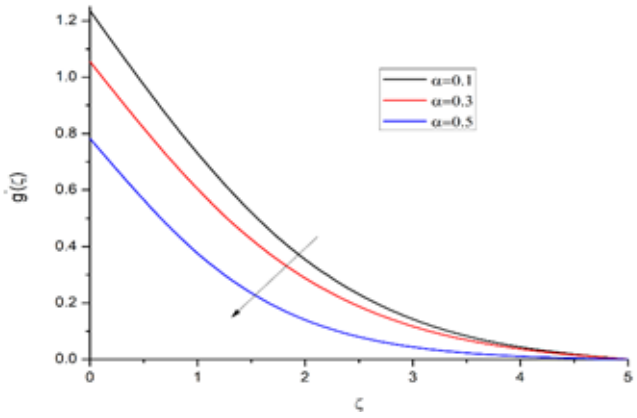

Figure 20. Effect of α (ratio parameter) on $g^{'}(\varsigma)$.

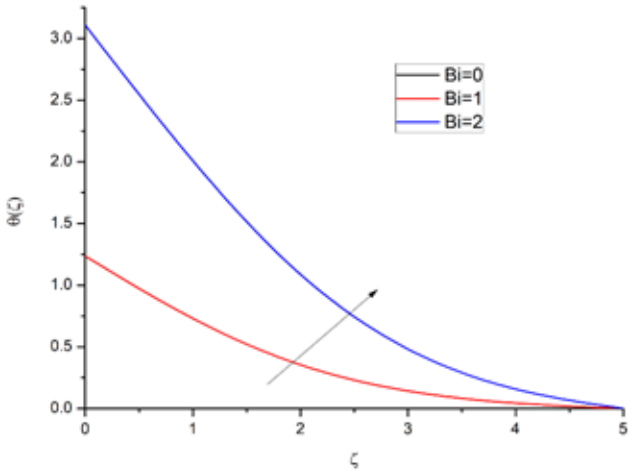

Figure 21. Effect of Bi (Biot number) on $\varphi(\varsigma)$.

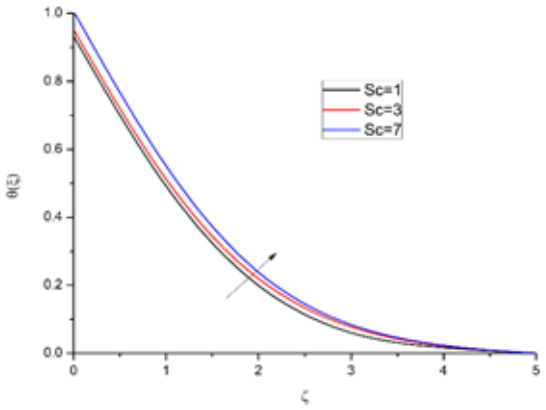

Figure 22. Effect of Sc (Schmidt number) on $\theta(\varsigma)$.

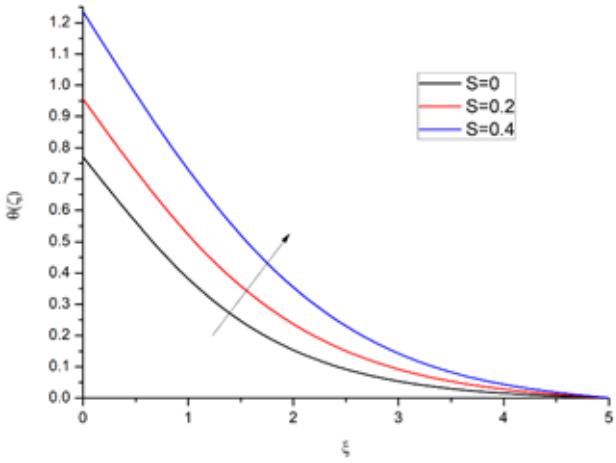

Figure 23. Effect of S (heat generation/absorption parameter) on $\theta(\varsigma)$.

4.0 Discussion on Graphs

Figure 1 and 2 manifest the effect of the Forchheimer number on velocities. Velocity reduces with the rise in Forchheimer number as the permeability of the porous medium increases, thus flow rate decreases. Figure 3 shows temperature variation under the impact of the Forchheimer number. It increases as the value of the Forchheimer number rises. Temperature enhances with the developing value of the Forchheimer number since fluid flow is hampered due to the porous medium. Figure 4 shows the variation in temperature for the Prandtl number. Temperature decreases with the growing value of the Prandtl number. Prandtl number relates kinematic viscosity with thermal diffusivity, which connects the velocity boundary layer to the thermal boundary layer. The smaller the Prandtl number, the more thermal diffusivity. Figure 5 shows variation in temperature concerning radiation parameter. The temperature rises with a rise in radiation parameter value as the coefficient of absorption coefficient decreases. Thus, there is an increase in radiative heat flux, which shows an increase in thermal radiation parameter. Figure 6 shows temperature variation concerning thermophoresis. Temperature declines as thermophoresis parameter decline. Temperature gradient increases; hence, the difference between ambient and surface temperature increases due to which nanoparticles are suspended in fluid.

Figures 7 and 8 show alterations in velocities $f'(\varsigma)$ and $g'(\varsigma)$ with the magnetic parameter. It decreases with a rise in magnetic parameter value due to the presence of Lorentz force. The density of fluid decreases, due to which the clash between nanoparticles reduces. Hence, velocity decreases in both directions. Figures 9 and 10 manifest the effect of the permeability parameter on velocities. Velocities show opposite behaviour with permeability parameter since fluid-particle interaction is less. Figure 11 shows the impact of the permeability parameter on temperature. Temperature grows with permeability parameter development, since slow motion leads to temperature improvement and hence the thermal boundary film. Figure 12 exhibits the behaviour of the λ, permeability parameter on concentration. At a distance of two units from the origin, concentration reduces and accelerates as increased permeability parameter allow fluids to pass quickly.

Figure 13 shows the variation in concentration for the Brownian motion parameter. First concentration profile rises to two units from the origin, then declines. Nanofluid particles experience more force hence, travel in the reverse direction due to an increase in Brownian motion parameter. Figure 14 depicts concentration variation with chemical reaction parameter. First concentration profile expands up to some distance, then shows the opposite behaviour and contracts. Figures 15 and 16 demonstrate the impression of the temperature ratio parameter and activation energy on concentration. Up to a certain distance from the origin, it rises and then the behaviour of the concentration profile changes and shows a downfall. Figures 17 and 18 illustrate the consequences of the rate constant and chemical reaction order onto concentration. Up to some distance from

Table 1. The skin friction coefficient for the different parameter value

λ	F_r	α	$C_{fx}\,\mathrm{Re}_y^{\frac{1}{2}}$	$C_{fy}\,\mathrm{Re}_y^{\frac{1}{2}}$
	0.5	0.3	1.372592	1.674593
0.4			1.367893	1.845679
0.6			1.389997	1.954328
0.2	0		1.413457	1.457689
	0.5		1.394214	1.954468
	1		1.409648	1.964458
	2		1.378946	2.548743
0.4	0.5	0.1	1.378884	1.969966
		0.3	1.392228	1.85675
		0.5	1.4	1.745679
0.6	0.5	0.1	1.360045	1.945222
		0.3	1.385378	1.758883

Table 2. Nusselt number corresponding to different parameter values for linearly stretching sheet

λ	Fr	α	γ	Nt	Nb	Pr	Sc	Hayat,t et.al 2017 $Re_x^{-1/2}Nux$	Hazmad et 2021 $Re_x^{-1/2}Nux$	Present Result when a=0 $Re_x^{-1/2}Nux$
0.0	0.1	0.2	0.3	0.2	0.5	1.0	1.0	0.20448	0.204481	0.204484
0.2								0.20248	0.202481	0.202489
0.5								0.1997	0.199702	0.199704
0.2	0.0	0.2	0.3	0.2	0.5	1.0	1.0	0.20278	0.202782	0.202786
	0.2							0.2022	0.202203	0.202204
	0.4							0.20164	0.201644	0.201644
0.2	0.1	0.0	0.3	0.2	0.5	1.0	1.0	0.19458	0.194583	0.194588
		0.3						0.2056	0.205601	0.205607
		0.5						0.2108	0.210802	0.210808
0.2	0.1	0.2	0.2	0.2	0.5	1.0	1.0	0.15148	0.151482	0.151486
			0.5					0.27696	0.276963	0.276965
			1.0					0.38194	0.381939	0.381941
0.2	0.1	0.2	0.3	0.0	0.5	1.0	1.0	0.20306	0.203058	0.203060
				0.5				0.20159	0.201591	0.201598
				1.0				0.20004	0.200038	0.200040
0.2	0.1	0.2	0.3	0.2	0.5	1.0	1.0	0.20248	0.202481	0.202480
					1.0			0.20248	0.202481	0.202485
					1.5			0.20248	0.202482	0.202485
0.2	0.1	0.2	0.3	0.2	0.5	0.5	1.0	0.16685	0.166854	0.166880
						1.0		0.20248	0.202482	0.202489
						1.5		0.21949	0.219493	0.219499
						1.0	0.5	0.20271	0.202712	0.202715
							1.0	0.20248	0.202483	0.202490

the origin, there is growth in the concentration profile, then decay. As concentration decreases, the number of molecules participating in chemical reactions decreases.

Figures 19 and 20 show alterations in velocities with the ratio parameter and temperature with suction parameter. Ratio parameter and velocity show opposite behaviour.

Table 3. Nusselt number corresponding to different parameter values for quadratically stretching sheet

λ	F_r	α	γ	N_b	N_t	Pr	Sc	$-Nu_x Re_x^{\frac{-1}{2}}$
0.2		0.1	0.2	0.5	0.5	2	1	0.501256
0.4								0.499124
0.6								0.453782
0.2	0.5	0.1	0.2	0.5	0.5	2	1	0.519863
	1							0.468882
	2							0.484456
0.2	0.5	0.1	0.2	0.5	0.5	2	1	0.492226
		0.3						0.478893
		0.5						0.503378
0.2	0.5	0.3	0.2	0.5	0.5	2	1	0.502217
			0.4					0.516689
			0.6					0.499994
0.2	0.5	0.3	0.2	0.4	0.5	2	1	0.487745
				0.5				0.492658
				0.6				0.508769
0.2	0.5	0.3	0.2	0.5	0.4	2	1	0.503368
					0.5			0.487659
					0.7			0.475996
0.2	0.5	0.3	0.2	0.5	0.5	2	1	0.486665
						3		0.502235
						4		0.525678
0.2	0.5	0.3	0.2	0.5	0.5	2	1	0.478944
							3	0.489995
							7	0.500032

Reverse behaviour is observed in both directions as the ratio parameter is b/a. If the denominator increases, then the numerator decreases and vice-versa. Figures 21 and 22 depict the effect of Biot number Bi and Schmidt number Sc on temperature. The temperature rises with a higher value of the Biot number and Schmidt number. Schmidt number is the ratio of thermal diffusivity to mass diffusion. The higher the Schmidt number more thermal diffusivity, hence the increase in the temperature profile. Figure 23 presents the effect of heat generation/absorption parameter on temperature. The temperature expands with an increase in heat generation/absorption parameter. Nanofluid can retain temperature for a long time, hence slighter heat transfer.

The skin friction coefficient is calculated for different values of , λ and α and shown in Table 1. Nusselt number for a linearly stretching sheet is compared with previous work done by Hayat *et al.*[27] and Alotaibi & Eid[36] and presented in Table 2. Result holds good for present work. Nusselt number for a quadratically stretching sheet is calculated corresponding to different parameters values and shown in Table 3

5.0 Conclusions

This work is dedicated to examining the 3-dimensional motion of nanofluid through Darcy –Forchheimer porous medium accompanying heat radiation, chemical reaction, thermal source/sink and magnetic field. The effect of the thermophoresis parameter (N_t) and Brownian motion (N_b) parameter is also considered in examining temperature and concentration profiles. A nonlinear system of differential equations is solved using MAPLE software. The following are the significant findings:

- Velocity $f'(\varsigma)$ and $g'(\varsigma)$ decreases with a rise in the magnetic parameter, Darcy-Forchheimer number and permeability parameter value. In contrast, an increment in the ratio parameter leads to a decay in velocity $f'(\varsigma)$ and an increment in velocity $g'(\varsigma)$.

- The temperature grows with an increment of radiation parameter R_d), Darcy-Forchheimer number F_r, thermophoresis parameter N_t, permeability parameter λ, Biot number Bi, Schmidt number Sc and heat generation/absorption

parameter S value. In contrast, a rise in the Prandtl number Pr shows decrement in temperature

- The concentration profile first reduces and then accelerates for the permeability parameter, Brownian motion parameter, chemical reaction parameter, temperature ratio parameter, fitted rate constant and order of the chemical reaction, whereas behaviour is opposite with activation energy.
- The research reveals some insight on nanomaterials flow like Al, Cu, Ag, Au, Fe, metal oxide (Al_2O_3, CuO, TiO_2), metal carbide (SiC), Nitride (AlN, SiN), layered (Al+ Al_2O_3, Cu + C), carbon materials (CNTs, diamond, graphite) and also thermal variations for forced convection.

6.0 Acknowledgement

Authors SY and RKR are thankful to Ramaiah Institute of Technology, India, for providing financial assistance to carry out this research work.

7.0 References

1. Choi SUS. Enhancing thermal conductivity of fluids with nanoparticles. ASME. 1995; 66:99-105.
2. Buongiorno J. Convective Transport in Nanofluids. Journal of Heat Transfer. 2006; 128(3):240–250. https://doi.org/10.1115/1.2150834
3. Makinde OD, Chinyoka T. MHD transient flows and heat transfer of dusty fluid in a channel with variable physical properties and Navier slip condition. Computers & Mathematics with Applications. 2010; 60(3):660–669. https://doi.org/10.1016/j.camwa.2010.05.014
4. Gireesha BJ, Mahanthesh B, Manjunatha PT, Gorla RSR. Numerical solution for hydromagnetic boundary layer flow and heat transfer past a stretching surface embedded in non-Darcy porous medium with fluid-particle suspension. Journal of the Nigerian Mathematical Society. 2015; 34(3):267–285. https://doi.org/10.1016/j.jnnms.2015.07.003
5. Muhammad T, Alsaedi A, Hayat T, Shehzad SA. A revised model for Darcy-Forchheimer three-dimensional flow of nanofluid subject to convective boundary condition. Results in Physics. 2017; 7: 2791–2797. https://doi.org/10.1016/j.rinp.2017.07.052
6. Rasool G, Shafiq A, Baleanu D. Consequences of Soret–Dufour effects, thermal radiation, and binary chemical reaction on Darcy Forchheimer flow of nanofluids. Symmetry. 2020; 12(9):1421. https://doi.org/10.3390/sym12091421
7. Eid MR, Mabood F. Two-phase permeable non-Newtonian cross-nanomaterial flow with Arrhenius energy and entropy generation: Darcy-Forchheimer model. Physica Scripta. 2020; 95(10): 105209. https://doi.org/10.1088/1402-4896/abb5c7.
8. Hosseinzadeh, K, Gholinia M, Jafari B, Ghanbarpour, A, Olfian H, Ganji DD. Nonlinear thermal radiation and chemical reaction effects on Maxwell fluid flow with convectively heated plate in a porous medium. Heat Transfer-Asian Research. 2019; 48(2):744–759. https://doi.org/10.1002/htj.21404
9. Vedavathi N, Venkatadri K, Gaffar SA, Dharmaiah G. Entropy analysis of magnetohydrodynamic nanofluid transport from an inverted cone: Buongiorno's model. Nanoscience and Technology: An International Journal. 2021; 12(4):81–103. https://doi.org/10.1615/NanoSciTechnolIntJ.2021035659
10. Vidya Shree V, Rudresha C, Balaji C, Maruthamanikandan S. Effect of MFD viscosity on ferroconvection in a fluid saturated porous medium with variable gravity. Journal of Mines, Metals and Fuels. 2022; 70(3A):98-103.
11. Crane LJ. Flow past a stretching plate. Zeitschrift Für Angewandte Mathematik Und Physik ZAMP. 1970; 21(4):645–647. https://doi.org/10.1007/BF01587695
12. Khan WA, Pop I. Boundary-layer flow of a nanofluid past a stretching sheet. International Journal of Heat and Mass Transfer. 2010; 53(11–12):2477–2483. https://doi.org/10.1016/j.ijheatmasstransfer.2010.01.032
13. Makinde OD, Aziz A. Boundary layer flow of a nanofluid past a stretching sheet with a convective boundary condition. International Journal of Thermal Sciences. 2011; 50(7):1326–1332. https://doi.org/10.1016/j.ijthermalsci.2011.02.019
14. Cortell R. Effects of viscous dissipation and radiation on the thermal boundary layer over a no linearly stretching sheet Physics Letters A. 2008; 372(5):631–636. https://doi.org/10.1016/j.physleta.2007.08.005
15. Prasad KV, Santhi SR, Datti PS. Non-Newtonian power-law fluid flow and heat transfer over a nonlinearly stretching surface. Applied Mathematics. 2012; 03(05):425–435. https://doi.org/10.4236/am.2012.35065
16. Mukhopadhay S. Heat transfer analysis for unsteady MHD flow past a non-isothermal stretching surface. Nucl. Eng. Des. 2011; 241:4835-4839.
17. Vijaya Kumara VM, Aswatha, Banu Prakash Reddy V, Amit Datta D, Balaji V, Ashik AV. A numerical investigation of natural convection in a porous enclosure

with lower wall heating. Journal of Mines, Metals and Fuels. 2023; 70(10A):195–201. https://doi.org/10.18311/jmmf/2022/31225

18. Srinvasulu T, Bandari S. MHD boundary layer flow of nanofluid over a nonlinear stretching sheet with effect of non-uniform heat source and chemical reaction. Journal of Nanofluids. 2017; 6(4):637–646. https://doi.org/10.1166/jon.2017.1362
19. Elgazery NS. Nanofluids flow over a permeable unsteady stretching surface with non-uniform heat source/sink in the presence of inclined magnetic field. Journal of the Egyptian Mathematical Society. 2019; 27(1). https://doi.org/10.1186/s42787-019-0002-4
20. Jafar AB, Shafie S, Ullah I. MHD radiative nanofluid flow induced by a nonlinear stretching sheet in a porous medium. Heliyon. 2020; 6(6):e04201. https://doi.org/10.1016/j.heliyon.2020.e04201
21. Saeed A, Kumam P, Nasir S, Gul T, Kumam W. Nonlinear convective flow of the thin film nanofluid over an inclined stretching surface. Scientific Reports. 2021; 11(1). https://doi.org/10.1038/s41598-021-97576-x
22. Rasool G, Shafiq A, Alqarni MS, Wakif A, Khan I, Bhutta MS. Numerical scrutinization of Darcy-Forchheimer relation in convective magnetohydrodynamic nanofluid flow bounded by nonlinear stretching surface in the perspective of heat and mass transfer. Micromachines. 2021; 12(4):374. https://doi.org/10.3390/mi12040374
23. Abbas N, Rehman KU, Shatanawi W, Malik MY. Numerical study of heat transfer in hybrid nanofluid flow over permeable nonlinear stretching curved surface with thermal slip. International Communications in Heat and Mass Transfer. 2022; 135:106107. https://doi.org/10.1016/j.icheatmasstransfer.2022.106107
24. Darcy HPG. Les Fontaines publiques de la Ville de Dijon: exposition et application des Principes à suivre et des formules à employer dans les questions de distribution d'eau, etc; Dalamont: Springtown, TX, USA, 1856.
25. Whitaker S. The Forchheimer equation: A theoretical development. Transport in Porous Media. 1996; 25(1):27–61. https://doi.org/10.1007/BF00141261
26. Sowbhagya. Outlook of density maximum on the onset of Forchheimer-Bénard convection with through flow. Journal of Mines, Metals and Fuels. 2022; 70(8A):32–40. https://doi.org/10.18311/jmmf/2022/32007
27. Hayat T, Aziz A, Muhammad T, Alsaedi A. Darcy–Forchheimer Three-dimensional flow of Williamson nanofluid over a convectively heated nonlinear stretching surface. Communications in Theoretical Physics. 2017; 68(3):387. https://doi.org/10.1088/0253-6102/68/3/387
28. Alzahrani AK, Ullah MZ, Alshomrani AS, Gul T. Hybrid nanofluid flow in a Darcy-Forchheimer permeable medium over a flat plate due to solar radiation. Case Studies in Thermal Engineering. 2021; 26:100955.
29. Muhammad R, Khan MI, Jameel M, Khan NB. Fully developed Darcy-Forchheimer mixed convective flow over a curved surface with activation energy and entropy generation. Computer Methods and Programs in Biomedicine. 2020; 188:105298. https://doi.org/10.1016/j.cmpb.2019.105298
30. Sulochana C, Prasanna Kumar T, Uma MS, Thulasi L. MHD Darcy-Forchheimer hybrid nanofluid flow past a nonlinear stretching surface: Numerical study. IOP Conference Series: Materials Science and Engineering. 2021; 1145(1):012042. https://doi.org/10.1088/1757-899X/1145/1/012042
31. Muhammad T, Alsaedi A, Hayat T, Shehzad SA. A revised model for Darcy– Forchheimer three-dimensional flow of nanofluid subject to convective boundary condition. Results Phys. 2017; 7:2791–2797.
32. Upreti H, Pandey AK, Kumar M, Makinde OD. Ohmic Heating and non-uniform heat source/sink roles on 3D Darcy–Forchheimer flow of CNTs nanofluids over a stretching surface. Arabian Journal for Science and Engineering. 2020; 45(9):7705–7717. https://doi.org/10.1007/s13369-020-04826-7
33. Mishra SR, Sharma RP, Tinker S, Panda GK. Impact of slip and the entropy generation in a Darcy-Forchhimer nanofluid past a curved stretching sheet with heterogeneous and homogenous chemical reactions. Journal of Nanofluids. 2022; 11(1):48–57. https://doi.org/10.1166/jon.2022.1813
34. Eid MR, Mahny KL, Al-Hossainy AF. Homogeneous-heterogeneous catalysis on electromagnetic radiative Prandtl fluid flow: Darcy-Forchheimer substance scheme. Surfaces and Interfaces. 2021; 24:101119. https://doi.org/10.1016/j.surfin.2021.101119
35. Sajid T, Sagheer M, Hussain S, Bilal M. Darcy-Forchheimer flow of Maxwell nanofluid flow with nonlinear thermal radiation and activation energy. AIP Advances. 2018; 8(3):035102. https://doi.org/10.1063/1.5019218
36. Alotaibi H, Eid MR. Thermal analysis of 3D electromagnetic radiative nanofluid flow with suction/blowing: Darcy–Forchheimer scheme. Micromachines. 2021; 12(11):1395. https://doi.org/10.3390/mi12111395
37. Shobha KC, Patil Mallikarjun B. Effect of Nonlinear thermal radiation on flow of Williamson nanofluid in a vertical porous channel with heat source or sink by using adomian decomposition method. Journal of Nanofluids. 2022; 11(1):39–47. https://doi.org/10.1166/jon.2022.1822

38. Patil PM, Doddagoudar SH, Shankar HF. Influence of nonlinear thermal radiation on mixed convective hybrid nanofluid flow about a rotating sphere. Heat Transfer. 2022; 51(6):5874–5895. https://doi.org/10.1002/htj.22573
39. Ullah H, Alsubie A, Fiza M, Hamadneh NN, Islam S, Khan I. Impact of hall current and nonlinear thermal radiation on Jeffrey nanofluid flow in rotating frame. Mathematical Problems in Engineering. 2021; 1–21. https://doi.org/10.1155/2021/9930017
40. Jaafar A, Waini I, Jamaludin A, Nazar R, Pop I. MHD flow and heat transfer of a hybrid nanofluid past a nonlinear surface stretching/shrinking with effects of thermal radiation and suction. Chinese Journal of Physics. 2022; 79:13–27. https://doi.org/10.1016/j.cjph.2022.06.026
41. Ali H, Soleimani H, Yahya N, Khodapanah L, Sabet M, Demiral BMR, Hussain T, Adebayo LL. Enhanced oil recovery by using electromagnetic-assisted nanofluids: A review. Journal of Molecular Liquids. 2020; 309, 113095. https://doi.org/10.1016/j.molliq.2020.113095
42. Sheikhpour M, Arabi M, Kasaeian A, Rokn Rabei A, Taherian Z. Role of nanofluids in drug delivery and biomedical technology: methods and applications. Nanotechnology, Science and Applications. 2020; 13:47–59. https://doi.org/10.2147/NSA.S260374
43. Hasona W, Almalki N, ElShekhipy A, Ibrahim M. Combined effects of thermal radiation and magnetohydrodynamic on peristaltic flow of nanofluids: applications to radiotherapy and thermotherapy of cancer. Current Nanoscience. 2020; 16(1):121–134. https://doi.org/10.2174/1573413715666190318161351